

Supplementary information

Cyanide- and hydroxo-bridged nanocage: a new generation of magnetic coordination clusters.

*Abhishake Mondal,[†] Sonja Durdevik,[†] Lise-Marie Chamoreau,[†] Yves Journaux,[†] Miguel Julve,[§] Laurent
Lisnard,^{*†}, Rodrigue Lescouëzec^{*†}*

[†]Institut Parisien de Chimie Moléculaire (IPCM), UMR7201, UPMC Paris 6, 4 place Jussieu, 75252 Paris cedex5 (France);

[§]Instituto de Ciencia Molecular (ICMol), Facultad de Química, Universitat de València, Catedrático José Beltrán 2, 46980
Paterna, València (Spain).

Synthesis of **1**.

Crystal structure: data collection and refinement.

Table 1: Structural description of the Co₃ clusters.

Table 2: BVS calculations.

Table 3: Fe–C and Fe–N bond length distances in Å.

Figure S1a: representation of the {Co₃μ₃-OH} clusters with atom labels and BVS calculations for the oxygen atoms assuming cobalt(II). Top: Co(1) to Co(3). Bottom: Co(4) to Co(6).

Figure S1b: representation of the {Co₃μ₃-OH} clusters with atom labels and BVS calculations for the oxygen atoms assuming cobalt(II). Top: Co(7) to Co(9). Bottom: Co(10) to Co(12).

Fit of the magnetic data: details and comments.

Figure S2: *M* vs. *H/T* plot for **1**.

Synthesis of 1.

[PPh₄][Fe^{III}(Tp)(CN)₃].H₂O^[18] (70.3 mg, 0.1 mmol) and [Co₂(H₂O)(piv)₄(Hpiv)₄]^[13] (285 mg 0.3 mmol) were both dissolved in pure acetonitrile solution (8 mL). These two solutions were stirred and heated to about approx. 60°C for 1 hour, and the warm [Fe(Tp)(CN)₃]⁻ solution was then added dropwise into the [Co₂(H₂O)(piv)₄(Hpiv)₄] solution. The resulting purple solution was heated to approx. 60°C during one hour and finally filtered. Evaporation of the filtrate under ambient condition afforded X-ray suitable red prismatic crystals over 4 days. Yield: 0.314 g (65%). Elemental analysis calcd (%) for C₁₈₀H₂₇₉B₄Co₁₃Fe₄N₅₂O_{45.5}: C, 43.83; H, 5.70; N, 14.76; found: C, 43.76; H, 5.65; N, 14.60; selected IR vibration peaks (KBr/cm⁻¹, 300 K): $\nu = 2514$ (BH), 2160, (CN from Fe^{III}-CN-Co^{II}), 2102, 2074 (CN from Fe^{II}-CN-Co^{II}), 1594, 1550 (CO).

Crystal structure: data collection and refinement.

Crystal data for **1** (C₁₈₀H₂₇₉B₄Co₁₃Fe₄N₅₂O_{45.5}): red blocks, monoclinic, space group *Cc*, $a = 20.6791(7)$, $b = 36.3243(13)$, $c = 34.1575(12)$ Å, $\beta = 90.423(1)^\circ$, $V = 25656(2)$ Å³, $Z = 4$, $T = 200(2)$ K, $\rho = 1.277$ g.cm⁻³, $F(000) = 10248$, $\mu(\text{MoK}\alpha) = 1.105$ mm⁻¹. Data were collected on a Bruker Kappa APEX-II CCD diffractometer (MoK α , $\lambda = 0.71073$ Å). Crystals were mounted on a Hamilton cryoloop using Paratone-N oil and placed in the cold flow produced with an Oxford Cryocooling device. Partial hemispheres of data –predefined with the APEX II software [BrukerAXS Inc, Madison, Wisconsin, USA, 1998] – were collected using ϕ and ω scans. Integrated intensities were obtained with SAINT [BrukerAXS Inc, Madison, Wisconsin, USA, 1998] and were corrected for absorption with SADABS [BrukerAXS Inc, Madison, Wisconsin, USA; Blessing, R. H. *Acta Cryst.* **1995**, *A51*, 33]; The structure was solved by direct methods with SIR-92 [A. Altomare, G. Cascarano, C. Giacovazzo, A. Guagliardi, M. C. Burla, G. Polidori, M. Camalli *J. Appl. Cryst.* **1994**, *27*, 435.] and full-matrix least-squares refinement against F^2 was performed with the SHELXL [Sheldrick, G. M. *Acta Cryst.* **2008** *A64*, 112] to give, using 2576 parameters and 3 restraints, $wR_2 = 0.1346$ (55987 unique reflections), $R_1 = 0.0453$ (48048 reflections with $I > 2\sigma(I)$), $GOF = 1.034$, *Flack parameter* = -0.019(7). There is a quite large void (400 Å³) in the crystal structure, as underlined by Checkcif. There is residual density in this region and there must be missing solvent molecules in the proposed model. However, the low intensity of the residual peaks (<1 e.Å⁻³) prevented any sensible refinement. Moreover, the most important residues are located around the pivalates of the Co1-Co2-Co3 triangle, showing that the disorder of this part is not fully modelled. As mentioned above, no sensible model could be obtained. Some tertio-butyl moieties of pivalates are disordered over two positions and refined isotropically. CCDC 890505 contains the supplementary

crystallographic data for this paper. These data can be obtained free of charge via www.ccdc.cam.ac.uk/conts/retrieving.html (or from the Cambridge Crystallographic Data Centre, 12, Union Road, Cambridge CB2 1EZ, UK; fax: (+44) 1223-336-033; or deposit@ccdc.cam.ac.uk).

Table 1: Structural description of the Co₃ clusters.

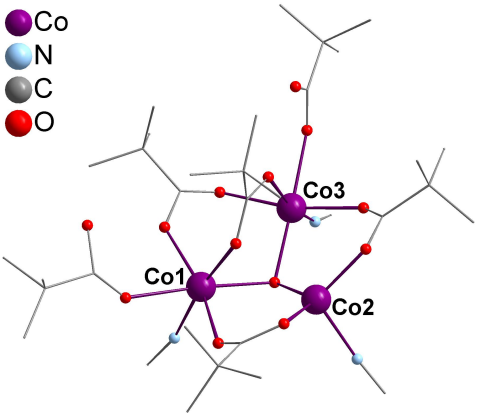
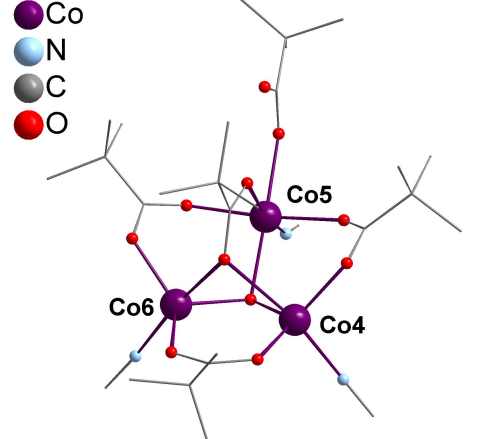
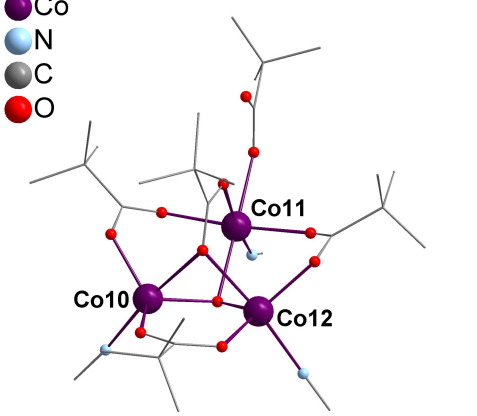
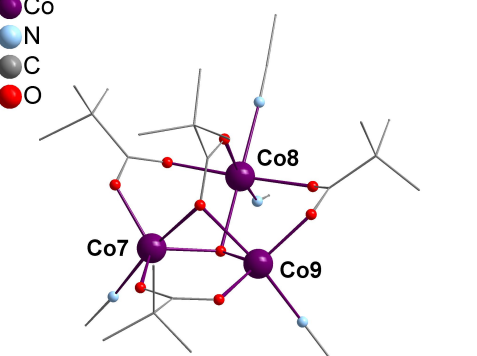
	<p>$[\text{Co}^{\text{II}}_3(\text{OH})(\text{piv})_4(\text{Hpiv})_2]^+$ {Co(1), Co(2), Co(3)}. 4 bridging pivalates, $\mu:\eta^1:\eta^1$. 2 terminal pivalic acids. 2 octahedral cobalt ions. 1 tetrahedral cobalt ion.</p>
	<p>$[\text{Co}^{\text{II}}_3(\text{OH})(\text{piv})_4(\text{Hpiv})]^+$ {Co(4), Co(5), Co(6)}. 4 bridging pivalates, three $\mu:\eta^1:\eta^1$ mode and one $\mu_3:\eta^2:\eta^1$. 1 terminal pivalic acid. 1 octahedral cobalt ion. 2 trigonal bipyramidal cobalt ions.</p>
	<p>$[\text{Co}^{\text{II}}_3(\text{OH})(\text{piv})_4(\text{Hpiv})]^+$ {Co(10), Co(11), Co(12)}. 4 bridging pivalates, three $\mu:\eta^1:\eta^1$ mode and one $\mu_3:\eta^2:\eta^1$. 1 terminal pivalic acid. 1 octahedral cobalt ion. 2 trigonal bipyramidal cobalt ions.</p>
	<p>$[\text{Co}^{\text{II}}_3(\text{OH})(\text{piv})_4(\text{MeCN})]^{1+}$ {Co(7), Co(8), Co(9)}. 4 bridging pivalates, three $\mu:\eta^1:\eta^1$ mode and one $\mu_3:\eta^2:\eta^1$. 1 terminal acetonitrile. 1 octahedral cobalt ion. 2 trigonal bipyramidal cobalt ions.</p>

Table 2: BVS calculations¹

<i>Atome Label</i>	<i>BVS calculated for Co(II)</i>	<i>BVS calculated for Co(III)</i>
Co(1)	1,9971	2,1326
Co(2)	1,8311	1,9892
Co(3)	2,0189	2,1489
Co(4)	1,8964	2,0516
Co(5)	1,9375	2,0636
Co(6)	1,8984	2,0476
Co(7)	1,8724	2,0160
Co(8)	1,9340	2,1344
Co(9)	1,9113	2,0620
Co(10)	1,8940	2,0491
Co(11)	1,9492	2,0796
Co(12)	1,9029	2,0411
Co(13)	1,8578	2,4344

¹ a) I. D. Brown, D. Altermatt, *Acta Crystallogr.* **1985**, *B41*, 244, b) N. E. Brese, M. O'Keeffe, *Acta Crystallogr.* **1991**, *B47*, 192, c) M. O'Keeffe, N. E. Brese, *Acta Crystallogr.* **1992**, *B48*, 152.

Table 3: Fe–C and Fe–N bond length distances in Å.

<i>Fe(III)</i>					
Fe(1)	C3	1.9256(40)	Fe(3)	C8	1.9147(37)
	C2	1.9270(41)		C9	1.9236(39)
	C1	1.9369(44)		C7	1.9299(37)
	N105	1.9644(35)		N304	1.9712(38)
	N101	1.9661(41)		N302	1.9752(35)
	N103	1.9775(40)		N300	1.9832(34)
<i>Fe(II)</i>					
Fe(2)	C4	1.8918(37)	Fe(4)	C10	1.8850(36)
	C6	1.8923(37)		C11	1.8861(38)
	C5	1.8942(38)		C12	1.8945(38)
	N203	2.0023(35)		N403	2.0102(36)
	N205	2.0100(34)		N401	2.0119(36)
	N201	2.0175(34)		N405	2.0152(35)

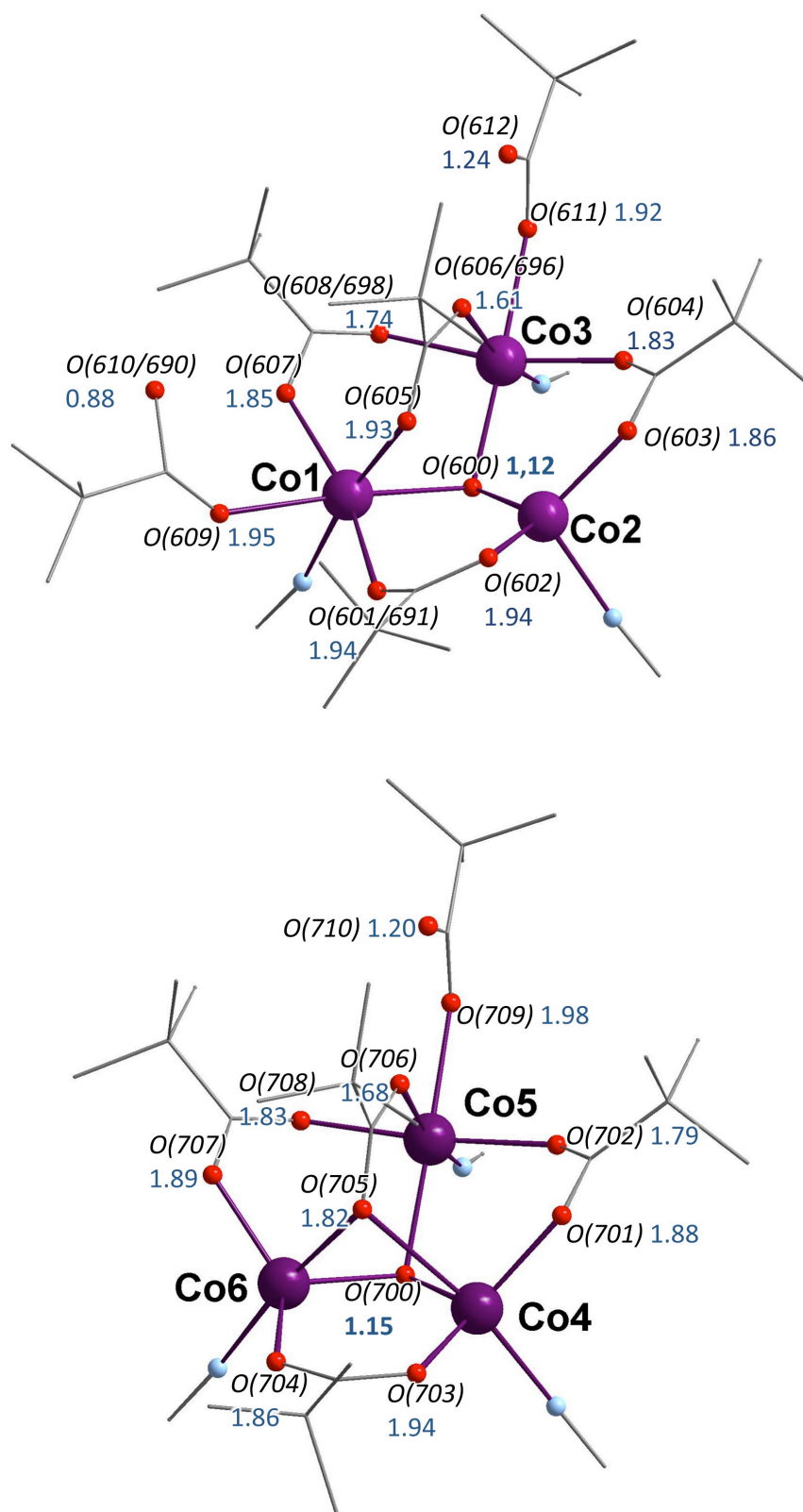


Figure S1a: representation of the {Co₃μ₃-OH} clusters with atom labels and BVS calculations for the oxygen atoms assuming cobalt(II). Top: Co(1) to Co(3). Bottom: Co(4) to Co(6).

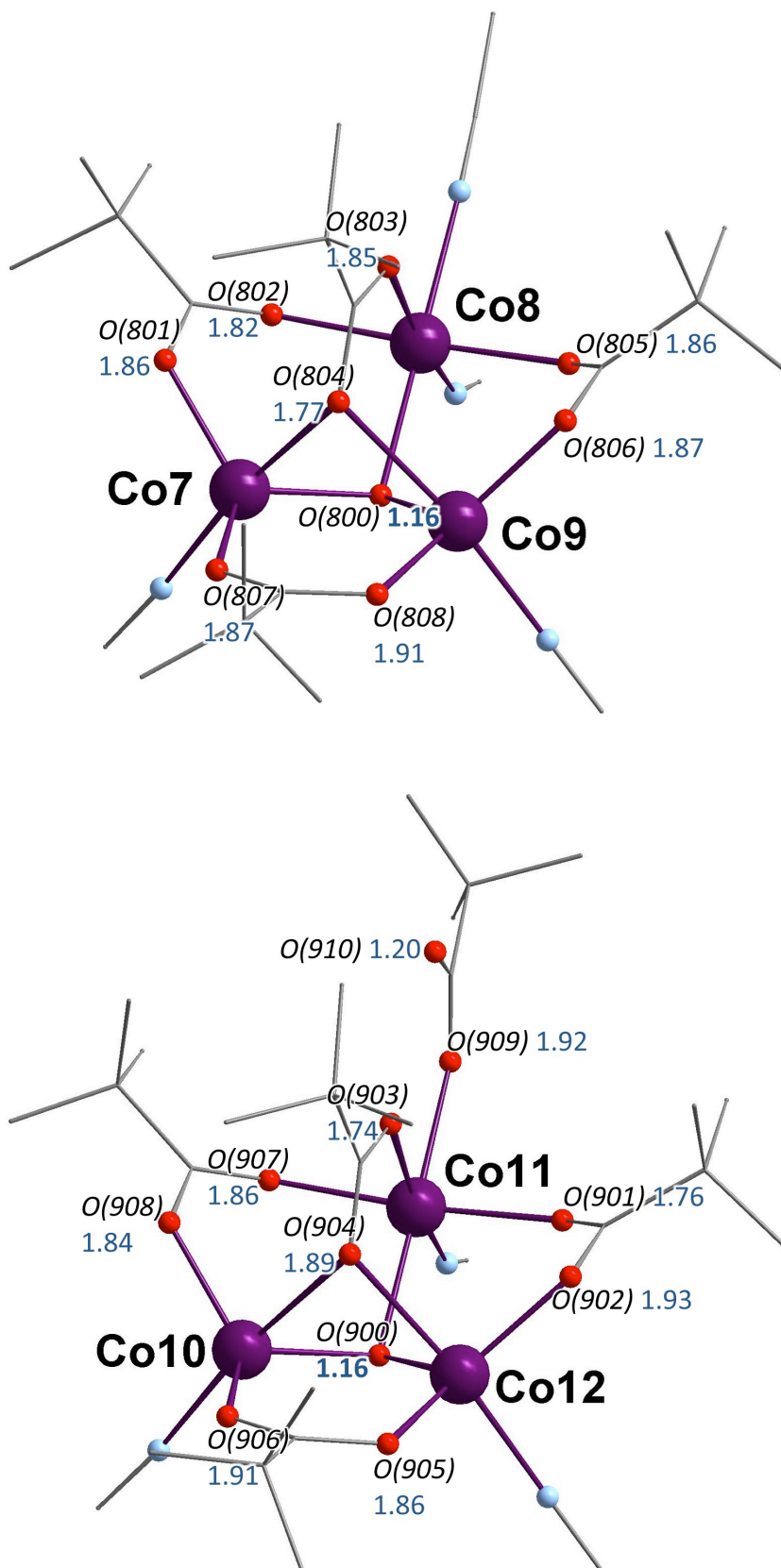


Figure S1b: representation of the {Co₃μ₃-OH} clusters with atom labels and BVS calculations for the oxygen atoms assuming cobalt(II). Top: Co(7) to Co(9). Bottom: Co(10) to Co(12).

Fit of the magnetic data: details and comments.

The system being composed of weakly coupled high-spin cobalt(II) ions and low-spin iron(III) ions, the magnetic data was modelled in the 300-50 K temperature range using the following Hamiltonian where the interaction between the magnetic ions are neglected [eq (1-3)]:

$$H = \sum_{i=1}^{13} H_{i \text{ Co}} + \sum_{j=1}^2 H_{j \text{ Fe}} \quad (1)$$

with

$$H_{iM} = v \alpha_M \lambda_M \mathbf{L} \cdot \mathbf{S} + D_M [\mathbf{L}_z^2 - 2/3] + \beta H [v \alpha_M \mathbf{L} + g_e \mathbf{S}] \quad (2)$$

The first term in the Hamiltonian (2) corresponds to the spin-orbit coupling effects, where λ_M with $M=\text{Co}, \text{Fe}$ is the spin-orbit coupling constant and α_M being the orbital reduction factor due to the existence of covalent character of bonds involving metal and ligands. The second term in this Hamiltonian accounts for the axial distortion of the six-coordinated Co^{II} or Fe^{III} ions. The last term represents the Zeeman interaction. The numerical coefficient v depends on electronic configuration and comes from the isomorphic transformation which convert the hamiltonian for a $^{2S+1}T_2$ or $^{2S+1}T_1$ state into an hamiltonian for a ^{2S+1}P term ($L=1$). For high-spin cobalt(II) and low-spin iron(III) these coefficients are equal to $v = -3/2$ and $v = -1$ respectively. [1]

Adding a TIP term to take into account the effect of unpopulated excited states, the least-squares fit of the experimental data of **1** using full diagonalisation of the Hamiltonian matrix performed in the 300–50 K temperature range led to $\lambda_{\text{Co}} = -120 \text{ cm}^{-1}$, $D_{\text{Co}} = 468 \text{ cm}^{-1}$, $\alpha_{\text{Co}} = 0.81$, $\lambda_{\text{Fe}} = -372 \text{ cm}^{-1}$, $D_{\text{Fe}} = -324 \text{ cm}^{-1}$, $\alpha_{\text{Fe}} = 0.77$ and $\text{TIP} = 0.025 \text{ cm}^3 \text{ mol}^{-1}$. These values are in the expected range for high-spin cobalt(II) and low-spin iron(III) ions.

[1] R. M. Golding, *Applied wave mechanics* Van Nostrand Co, London, **1969** p 243.

Reduced magnetisation plot $M(H/T)$

The saturation magnetization value of 23.2 BM for **1** (figure S2) is close to the calculated one (25 BM) with the best parameters obtained by the fit of $\chi.T$ vs. T plot in the high temperature range. These reduced magnetisation M versus H/T curves are recorded in the 1.8K-8K temperature range where it is impossible to neglect the interaction between the magnetic ions as shown by the $\chi.T$ versus T plot. Given the size of the cluster (see ref 28), it is impossible to model these curves. However, the absence of a unique curve for the reduced variable H/T can have two origins. Firstly, the anisotropy of the iron and cobalt ions results in nonsuperposable isofield curves. Secondly, the exchange interactions through the cyanide and through the oxo bridges are quite weak (as observed in numerous previously reported Fe-CN-Co based systems, and, in agreement with the treatment of the $\chi.T$ vs. T plot). Thus numerous close-lying excited states lie close to the ground state, so that even at low temperature, the magnetization value results from a thermal distribution of various states. This distribution of close-lying levels also leads to nonsuperposable isofield curves.

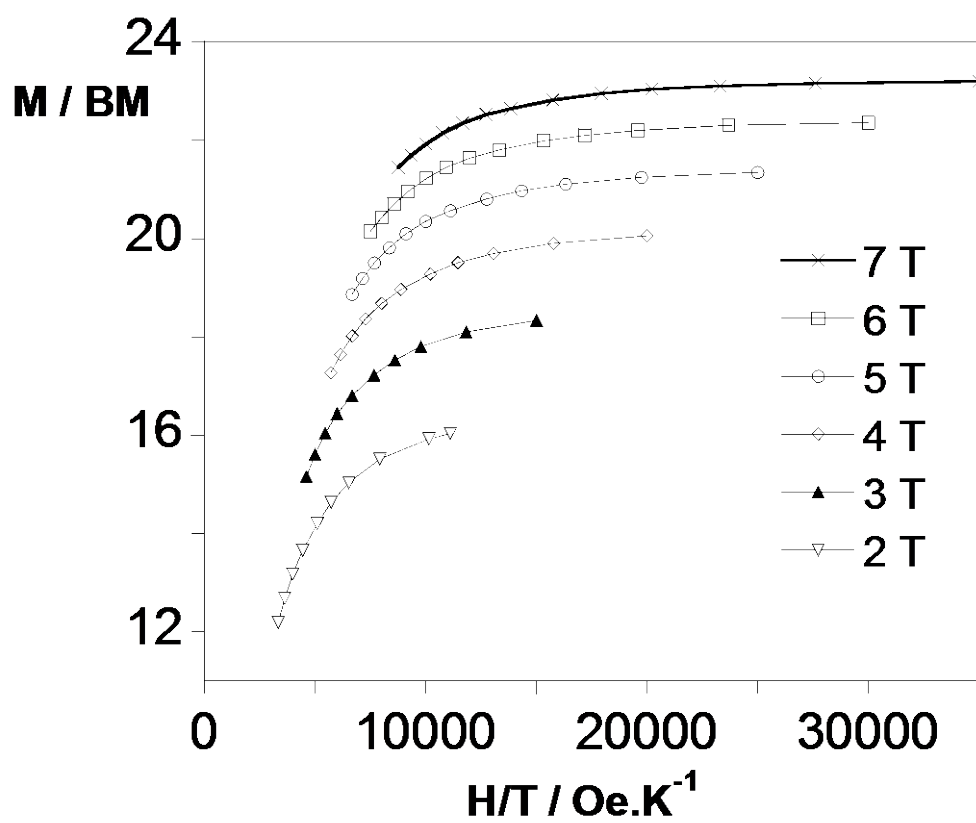


Figure S2: M vs. H/T plot for **1** (solid lines are eye guides).